Phosphorylation induces structural changes in the Autographa californica nucleopolyhedrovirus P10 protein

Farheen Raza,[a]* Joanna F. McGouran,[b]** Benedikt M. Kessler,[b] Robert D. Possee,[a] Linda A. King[a#]

Department of Biological & Medical Sciences, Oxford Brookes University, Oxford, UK[a]; Target Discovery Institute, Nuffield Department of Medicine, University of Oxford, Roosevelt Drive, Oxford OX3 7FZ, UK[b]

Running Head: Phosphorylation of AcMNPV P10

#Address correspondence to Linda A King, laking@brookes.ac.uk.

*Present address: Medical Research Council Toxicology Unit, Hodgkin Building, Lancaster Road, Leicester LE1 9HN, UK.

**Present address: School of Chemistry, Trinity College Dublin, University of Dublin, College Green, Dublin 2, Ireland

Word count for abstract: 195

Word count for rest of text: 5371

Structured Abstract

Abstract

Baculoviruses encode a variety of auxiliary proteins that are not essential for viral replication but provide them with a selective advantage in nature. P10 is a 10 kDa auxiliary protein produced in the very-late phase of gene transcription by Autographa californica multiple nucleopolyhedrovirus (AcMNPV). The P10 protein forms cytoskeletal-like structures in the host cell that associate with microtubules varying from filamentous forms in the cytoplasm to aggregated peri-nuclear tubules that form a cage-like structure around the nucleus. These P10 structures may have a role in the release of occlusion bodies (OBs) and thus mediate horizontal transmission of the virus between insect hosts. Here it is demonstrated, using mass spectrometric analysis, that the C-terminus of P10 is phosphorylated during virus infection of cells in culture. Analysis of the P10 mutants encoded by recombinant baculoviruses in which putative phosphorylation residues were mutated to alanine showed that serine 93 is a site of phosphorylation. Confocal microscopy examination of the serine 93 mutant structures revealed an aberrant formation of the peri-nuclear tubules. Thus, phosphorylation of serine 93 may induce aggregation of filaments to form tubules. Together, these data suggest that the phosphorylation of serine 93 affects P10 structural conformation.

Importance

The baculovirus P10 protein has been researched intensively since it was first observed in 1969, but its role during the viral infection remains unclear. It is conserved in the alphabaculoviruses and expressed at high levels during virus infection. Producing large amounts of a protein is wasteful for the virus unless it is advantageous for survival of its progeny and therefore P10 presents an enigma. As P10 polymerises to form organised cytoskeletal structures that co-localise

with the host cell microtubules, the structural relationship of the protein with the host cell may present a key to help understand the function and importance of this protein. This study addresses the importance of the structural changes in P10 during infection and how they may be governed by phosphorylation. The P10 structures affected by phosphorylation are closely associated with the viral progeny and thus, potentially, be responsible for its dissemination and survival.

Introduction

Autographa californica multiple nucleopolyhedrovirus (AcMNPV) is a model alphabaculovirus and belongs to the family of *Baculoviridae*. This family of viruses is characterised by a circular double-stranded DNA genome enclosed in a rod-shaped capsid and further enveloped by a membrane (1). The replication cycle of baculoviruses produces two forms of progeny virus: the budded virus (BV) and the occlusion-derived virus (ODV) (2, 3). The ODV is protected within a protein-rich matrix forming an occlusion body (OB) that is either polyhedral (nucleopolyhedroviruses) or granular (granuloviruses) in shape (4). Transcription of some baculovirus genes, notably *polyhedrin* (*ac8*) and *p10* (*ac137*), occurs in a very-late phase that initiates approximately six hours after the onset of late gene transcription (5). While the role of polyhedrin as an OB matrix protein is well-established, the P10 protein remains poorly understood. P10 is a 10 kDa protein that forms cytoskeletal-like fibrillar structures in virus-infected cells and together with polyhedrin accounts for the majority of the virus-encoded protein present in the host cell during the very-late phase (6).

71 Homologues of *p10* were reported in 27 alpha- and 2 beta-baculovirus genomes (7); however, we
72 found a further 25 homologues (19 alpha- and 6 beta-baculovirus) in the NCBI protein database
73 (Table 1).
74
75 Baculovirus replication can occur in the absence of P10 (8), but studies have indicated that P10
76 may have a number of roles in the very-late stages of the replication cycle (8–10). P10 has been
77 implicated in nuclear lysis as *Spodoptera frugiperda* cells infected with a recombinant AcMNPV
78 lacking *p10* failed to release OBs, even at two weeks post-infection (9). In contrast, cells infected
79 with the wild-type AcMNPV released large numbers of OBs at two days post-infection.
80
81 Early transmission electron microscopy (TEM) studies of the P10 protein structure reported a
82 close association between the polyhedron envelope (PE) and P10 (8–10). Virus infection of
83 *Trichoplusia ni* cells with an AcMNPV *p10* deletion mutant resulted in poor attachment of the
84 PE to the surface of polyhedra (9). Studies utilising scanning EM demonstrated that the
85 polyhedra from *Orgyia pseudotsugata* larvae infected with a *p10*-deficient recombinant O.
86 pseudotsugata (Op) MNPV had pitted surfaces, from dislodging of virions, whereas the wild-
87 type polyhedra had smooth surfaces (10).
88
89 Although P10 fibrillar structures have been described through TEM analyses dating from 1969
90 (11), immunofluorescence microscopy images first appeared in a study by Quant-Russell *et al*.
91 (12) . In OpMNPV-infected *Lymantria dispar* cells, P10 structures were first detected at 14 hpi
92 as 'fine threads' in the cytoplasm and by 16 hpi these structures had 'condensed into thicker rod-
93 like' structures that form an 'interconnected network' at later stages (12). Subsequent studies by
94 Patmanidi *et al*. (13) and Carpentier *et al*. (14) employed confocal immunofluorescence

95 microscopy to analyse P10 structures in AcMNPV-infected *S. frugiperda* and *T. ni* cells,
96 respectively. The P10 filamentous structures were evident at 18 hpi in AcMNPV-infected *T.ni*
97 cells (TN368 cell line), and these had formed a network in the cytoplasm by 30 hpi followed by
98 distinctive peri-nuclear aggregates or tubules by 36 hpi (14).
99
100 A study by Cheley *et al*. (15) revealed that *S. frugiperda* cells infected with a recombinant
101 AcMNPV encoding the catalytic subunit of *Aplysia* protein kinase A (PKA) developed cellular
102 projections. Analysis of these cells using TEM showed that these projections were a result of
103 extended microtubules (MTs). Moreover, [^{32}P] orthophosphate labelling of taxol-stabilised MTs
104 from cells infected with the PKA recombinant baculovirus showed high levels of phosphorylated
105 P10. However, no phosphorylated P10 was observed in MTs prepared from cells infected with
106 the wild-type virus. These data allowed the authors to conclude that the cellular projections were
107 a result of MT elongation induced by phosphorylated P10. Additionally, it was shown that P10
108 was phosphorylated by *Aplysia* PKA at the C-terminus. Further analysis of the virus-infected
109 cells revealed that phosphorylated P10 associated with MTs, but it could not bundle them.
110 Interaction of P10 with MTs during the wild-type virus infection was later confirmed in *S.*
111 *frugiperda* and *T. ni* cells (13, 14). These studies demonstrated that the initial P10 filamentous
112 structures in the cytoplasm co-align with MTs. Furthermore, formation of the P10 filamentous
113 structures was inhibited upon treatment with colchicine, which inhibits microtubule
114 polymerization (14). Together, these data suggest that P10's interaction with MTs is important
115 to its formation and stabilisation.
116
117 The work by Cheley *et al.,* (15) showed that phosphorylation of P10 by *Aplysia* PKA affected the
118 P10 structure. It is not known whether this phenomenon occurs in a wild-type AcMNPV

infection and in a natural AcMNPV host. In this study we provide evidence for P10 phosphorylation in AcMNPV infection of *T. ni* cells via mass spectrometric analysis and also identify the phospho-acceptor site within P10. The structural consequences of P10 phosphorylation were investigated through alanine mutagenesis and confocal microscopy.

Material and Methods

Cells and viruses

This study utilised cell lines derived from the ovary of *T. ni* (High Five™, TN368). TN368 (19) cells were grown in TC-100 Insect Medium (Gibco®) with 10% (v/v) fetal bovine serum (Sigma-Aldrich) as adherent culture. High Five™ (18) cells were grown in EX-CELL® 405 (Sigma-Aldrich) as suspension culture. Sf9 (16) and Sf21 (17) cells, derived from the ovary of *S. frugiperda,* were used in the process of recombinant baculovirus generation and plaque assay. Sf9 cells were grown in InsectExpress Sf9-S2 (PAA), and Sf21 cells in TC-100 Insect Medium (Gibco®) with 10% (v/v) fetal bovine serum (Sigma-Aldrich). Both Sf21 and Sf9 were maintained as suspension cultures. The wild-type virus used in this work was AcMNPV C6 (20).

Site-directed mutagenesis of *p10* and generation of recombinant viruses

In summary, site directed mutagenesis was performed using the QuikChange kit (Stratagene) according to the method described by Vandeyar *et al*. (21). In essence, DNA was synthesised in a PCR using a high fidelity *Pfu* DNA polymerase (Agilent Technologies) and custom primers. This was treated with *Dpn*I endonuclease to digest the parental DNA template. The *Dpn*I-treated

142 DNA was used to transform competent bacterial cells. All mutations were confirmed by DNA
143 sequencing.
144
145 The plasmid pCRII-TOPO-P10^{wt} was constructed by sub-cloning of the *p10* gene (amplified
146 from the AcMNPV strain C6) into pCRII-TOPO (Invitrogen) using the *Xba*I and *Eco*RI
147 restriction sites. The *p10* codons for serine 92 and 93 were then each mutated to specify alanine.
148 In the first step, serine 92 was mutated to alanine in a PCR reaction using P10_S92AF and
149 P10_S92AR primers (Table 2). In a second PCR reaction serine 93 was mutated to alanine using
150 P10_S93AF and P10_S93AR primers. The resulting plasmid was named pCRII-TOPO-
151 P10^{S9293A}.
152
153 The modified *p10* fragment was amplified from the plasmid pCRII-TOPO-P10^{S9293A} using
154 P10_S9293A_pBP8F and P10_S9293A_pBP8R primers in a PCR. The product was digested
155 with *Xba*I and *Xma*I and then sub-cloned into pBacPAK8, downstream of the polyhedrin
156 promoter, to generate pBacPAK8-P10^{S9293A}.
157
158 The plasmid pBacPAK8-P10^{S9293A} was used to generate single P10 mutants in which either
159 serine 92 or 93 codons were mutated to specify alanine instead. Single mutations were created
160 through site-specific mutagenesis using P10_S92A_pBP8F and P10_S92A_pBP8R primers to
161 derive pBacPAK8-P10^{S92A}, and P10_S93A_pBP8F and P10_S93A_pBP8R to derive
162 pBacPAK8-P10^{S93A}.
163

To generate a control, the *p10* gene was amplified from pCRIITOPO-P10^{wt} using P10_wtF and P10_wtR primers. The PCR product was digested with *Xba*I and *Xma*I and then sub-cloned into pBacPAK8 downstream of the polyhedrin gene promoter to derive pBacPAK8-P10^{wt}.

The plasmids pBacPAK8-P10^{S9293}, pBacPAK8-P10^{S92A}, pBacPAK8-P10^{S93A} and pBacPAK8-P10^{wt} were used in a co-transfection with *flash*BACULTRA genomic DNA (Oxford Expression Technologies Ltd) to generate recombinant viruses. These viruses were designated AcP10^{S9293A}, AcP10^{S92A}, AcP10^{S93A} and AcP10^{wt}, respectively.

To construct polyhedrin positive viruses, *p10* was amplified from the plasmid pBacPAK8-P10^{wt} using P10_wt_pW2BF and P10_wt_pW2BR primers in a PCR. The DNA product was digested with *Pst*I (this restriction site was introduced into the plasmid pAcUW2B through site-specific mutagenesis) and inserted into pAcUW2B, downstream of the *p10* promoter to derive pAcUW2B-P10^{wt}. This plasmid was then used to generate the *p10* mutants. The P10 residue, serine 93, was mutated to alanine through site-specific mutagenesis using P10_S93A_pW2BF and P10_S93A_pW2BR primers to derive pAcUW2B-P10^{S93A}.

To derive a pAcUW2B transfer vector encoding polyhistidine-tagged P10 (wild-type and serine 93 mutant), plasmids pAcUW2B-P10^{wt} and pAcUW2B-P10^{S93A} were used. The wild-type *p10* gene was PCR amplified from the plasmid pAcUW2B-P10^{wt} using HISP10_wt_pW2BF and HISP10_wt_pW2BR primers introducing a 6x histidine tag and a TEV cleavage site at the N-terminus. The PCR fragment and pAcUW2B were digested with *Pst*I and *Spe*I and ligated together to produce pAcUW2B-His-P10^{wt}. The serine 93 mutant *p10* was PCR amplified from the plasmid pAcUW2B-P10^{S93A} using HISP10_S93A_pW2BF and HISP10_S93A_pW2BR

primers introducing a 6x histidine tag and a TEV cleavage site at the N-terminus. The PCR fragment and pAcUW2B were digested with *Pst*I and *Spe*I; the fragment was then ligated into pAcUW2B, downstream of the *p10* promoter to derive pAcUW2B-His-P10^{S93A}. Recombinant viruses (AcUW2B-His-P10^{wt} and AcUW2B-His-P10^{S93A}) were generated as described above.

Generation of recombinant viruses

Cell cultures dishes (35 mm) were seeded with Sf9 cells at a density of $0.5x10^6$ ml^{-1}. Co-transfection mixtures were prepared using 1 ml of appropriate cell culture medium, 5 µl of Lipofectin® reagent (Invitrogen), 100 ng of *flash*BACULTRA™ (Oxford Expression Technologies Ltd) and 500 ng of transfer vector according to the method described by King and Possee (22). The medium containing the recombinant virus was collected on the fifth day. Viruses were amplified in Sf9 cell cultures and titres were determined by plaque assay in plaque-forming units (pfu) ml^{-1}using Sf21 cells.

Immunofluorescence

For confocal immunofluorescence microscopy, TN368 cells were employed. These were seeded on glass coverslips (22 mm diameter) in 35 mm cell culture dishes at a density of $1x10^5$ ml^{-1} and were allowed to settle overnight at 28°C. To infect cells, the medium was removed from the dishes and 100 µl of appropriate dilution of the virus inoculum was added drop-wise onto the cells. For mock infection, 100 µl of cell culture medium was used. Cells were infected with each type of virus in triplicate. Cells were incubated at room temperature for 1 hour to allow virus adsorption. The inoculum was then removed and 2 ml of fresh media were added to the cells (this time point was defined as 0 hpi). Cells were incubated at 28°C until the desired time-point, medium was removed from the dishes and cells were washed twice with 1 ml of phosphate

212 buffered saline (PBS). For chemical fixation, cells were treated with 1 ml of 4% (v/v)
213 paraformaldehyde for 1 hour, washed once with 1 ml of PBS and stored at 4°C until required for
214 immunostaining.
215
216 Tubulin was stained using a mouse monoclonal anti-α-Tubulin antibody (Sigma-Aldrich) and an
217 anti-mouse Alexa Fluor 568 (Invitrogen). P10 was stained using a guinea pig polyclonal
218 antibody (13) and an anti-guinea pig Alexa Fluor 488 (Invitrogen). For immunofluorescence
219 staining, fixed cells were treated with a permeabilisation buffer (1% (w/v) bovine serum albumin
220 and 0.1% (v/v) Triton X-100 in PBS) for 10 minutes. Cells were washed with 1 ml of PBS
221 followed by 1 ml of 1% (w/v) BSA in PBS (PBS-BSA). Cells were probed with primary
222 antibody, diluted in PBS-BSA, for 50 minutes. Unbound antibody was removed by washing cells
223 with PBS-BSA three times. Cells were probed with secondary antibody diluted in PBS-BSA for
224 50 minutes and then washed three times with PBS. Following immunofluorescence staining,
225 coverslips were mounted on glass slides using the Vectashield mounting media (Vector
226 Laboratories). Coverslips were sealed using a clear nail varnish and slides were stored at 4°C
227 protected from light.
228
229 **Confocal microscopy**
230 Confocal laser scanning microscopy of immunostained cells was performed using the Zeiss LSM
231 510 META system with an Axio Imager-Z1 upright microscope. Images were acquired using the
232 oil immersion objectives EC Plan-Neofluar 40x (1.3 numerical aperture) or Plan-Apochromat
233 63x (1.4 numerical aperture). A multi-track setup was employed to prevent signal cross-over.
234 Fluorescence from Alexa Fluor 488 and Alexa Fluor 568 was recorded through the laser lines
235 488- and 543 nm, respectively. Projection 3D images were generated using the Zeiss LSM Image

Browser (v4.2). Images shown were selected to be representative from a large number of individual cells examined (n>100).

Mass spectrometry

Coomassie stained protein gel bands of P10 were excised and cut into small pieces (1–2mm^3) and transferred to a 1.5 ml tube. Gel pieces were shaken vigorously for 18 hours in destaining solution (1ml, 50% (v/v) methanol, 5% (v/v) acetic acid). Further destaining was carried out for 2-3 hours with fresh destaining solution. The destaining solution was removed and gel pieces were dehydrated in 200 µl of acetonitrile for 5 minutes. Acetonitrile was removed and the dehydration step repeated. Reduction was carried out with 30 µl of 10 mM dithiothreitol buffer for 30 minutes. Reduction buffer was removed and replaced with alkylation buffer; alkylation was carried out with 30 µl of 50 mM iodoacetamide buffer for 30 minutes. Alkylation buffer was removed and gel pieces were dehydrated in 200 µl acetonitrile for 5 minutes. Acetonitrile was removed and gel pieces were rehydrated in 200 µl of 100 mM ammonium bicarbonate solution for 10 minutes. The dehydration step was repeated with 200 µl acetonitrile for 5 minutes and the solution was removed.

Digestion was carried out using a *Staphylococcus aureus* protease V8, endoproteinase GluC (NEB) which was prepared by adding 1 ml of ice-cold 50 mM ammonium bicarbonate to 20 µg of GluC (final concentration 20 ng/µl). Gel pieces were rehydrated with 30 µl of GluC solution on ice for 10 minutes and then briefly centrifuged to allow removal of excess enzyme solution. After adding 5 µl of 50 mM ammonium bicarbonate buffer solution to the gel pieces, digestion was performed at 37 °C for 18 hours.

Peptides were extracted from the gel pieces during each of the three successive 10 minute incubations of: (1) 50 µl of 50 mM ammonium bicarbonate buffer, (2) 50 µl of extraction buffer 1 (50% (v/v) acetonitrile, 5% (v/v) formic acid) and (3) 50 µl of extraction buffer 2 (85% (v/v) acetonitrile, 5% (v/v) formic acid). The peptide solution was dried completely in a vacuum centrifuge and resuspended in 20 µl of a buffer solution (2% (v/v) acetonitrile, 0.1% (v/v) formic acid).

For matrix assisted laser desorption/ionization time-of-flight (MALDI-TOF) mass spectrometry analysis, 1 µl of peptide solution was mixed with 1 µl of matrix (α-cyano-4-hydroxycinnamic acid) and spotted on a MALDI target. Samples were measured by MALDI-TOF (Ultraflex™, Bruker Daltonics) in linear mode. The MALDI-TOF spectra were analysed using the flexAnalysis software (Bruker Daltonics).

Protein purification

A shaking suspension culture of *T. ni* High Five™ cells was set up at a density of $0.5x10^6$ cells ml^{-1}in a total volume of 500 ml. Cells were infected with the virus expressing the His-tagged protein at an MOI of 5 and incubated at 28°C. At the required time-point, cells were harvested by centrifugation at 10,000 x*g* for 15 minutes. The supernatant was removed and cells were washed with 50 ml of ice-cold PBS. Cells were lysed with a CytoBuster™ Protein Extraction Reagent (Novagen) and spun at 14,000 x*g* for 30 minutes to remove all insoluble material. After centrifugation, supernatant was filtered through a 0.45 µm membrane to prevent clogging of purification resin in subsequent steps. His-tagged protein purification was carried out using the His-Bind® purification kit (Novagen) according to the manufacturer's instructions. In brief, an iminodiacetic acid (IDA) agarose resin was used in a spin column to purify His-tagged proteins.

The IDA agarose resin was activated with a charge buffer (50 mM $NiSO_4$) and equilibrated with a binding buffer (0.5 M NaCl, 20 mM Tris-HCl, 5 mM imidazole, pH 7.9). Prepared soluble lysates were passed through the spin column. The resin was treated with the binding buffer and then wash buffer (0.5 M NaCl, 60 mM imidazole, 20 mM Tris-HCl, pH 7.9) to remove any non-specific binding of proteins with the resin. Elution was performed with the buffer containing 400 mM imidazole, 0.5 M NaCl, 20 mM Tris-HCl at pH 7.9. Purified protein was assessed for purity through Coomassie staining.

Circular Dichroism

Circular dichroism (CD) spectra were recorded on a Jasco J-720 spectropolarimeter (Jasco GmbH) using a 0.05 cm path length quartz cell. Spectra of a 100 μg ml^{-1} protein solution in 10 mM phosphate buffer were averaged from 4 to 16 scans (260–190 nm) and corrected using a buffer blank. The CD spectra were analysed on the CD analyser system (V2.02) software using the LINCOMB method (23).

Results

1. Temporal analysis of P10 structures by confocal microscopy

Wild-type AcMNPV P10 structures in virus-infected cells were analysed by laser scanning confocal microscopy to visualise the major changes that occur from their peak expression time at 48 hpi (24) until they are semi-disintegrated, typically at 96 hpi (Figure 1), extending previous studies which examined P10 structures until 72 hpi (14). TN368 cells were infected in triplicate culture dishes with AcMNPV at a multiplicity of infection (MOI) of 10 pfu $cell^{-1}$, fixed at 48-, 72- and 96 hpi, and then immunostained to detect P10 and host MTs.

At 48 hpi (Fig. 1, left hand panels), P10 formed filamentous structures in the cytoplasm and around the nucleus of the host cell. Aggregated filaments were also observed surrounding the nucleus. The orientation of P10 filaments in the cytoplasm was similar to that of the host MTs and thus both were co-aligned, most prominently in regions of stable MTs. At 72 hpi (Fig. 1, centre panels), the P10 cytoplasmic filaments showed further bundling and were still co-aligned with MTs. At this time-point, thicker tubule-like structures, possibly resulting from aggregation of finer P10 filaments, were also observed surrounding the OB-filled nucleus. At 96 hpi (Fig. 1, right hand panels), the P10 peri-nuclear tubular structures had fully matured, and the cytoplasmic filaments were mostly detached and/or disintegrated. Some detached filaments had a loop-like terminal structure. Additionally, a layer of P10 was also observed enveloping the OBs inside the host nucleus at 72- and 96 hpi.

2. Phosphorylation of P10 in wild-type AcMNPV infection

This study utilised MALDI-TOF mass spectrometry to analyse changes in the mass of the P10 C-terminus that Cheley *et al*. (15) had reported to be the domain phosphorylated by *Aplysia* PKA. Analysis of the amino acid sequence of P10 showed that the C-terminus contained three potential phosphorylation sites at serine 70, 92 and 93. For MALDI-TOF analysis, *T. ni* cells were infected with wild-type AcMNPV at an MOI of 10 and harvested at 72 hpi. This time-point was selected as it showed both forms of P10 structures (Figure 1). Lysates were separated using SDS-PAGE and stained with Coomassie solution. Digestion of P10 protein was carried out using the endoproteinase GluC (*Staphylococcus aureus* protease V8) to cleave peptide bonds C-terminal to glutamic acid residues. The MALDI-TOF spectrum was analysed for peaks corresponding to the C-terminal peptide containing serine 92 and 93 residues.

Figure 2 shows a MALDI-TOF spectrum containing the m/z peaks (labelled) corresponding to the C-terminal peptide ^{82}LDSDARRGKRSSK^{94}, a product of the endoproteinase GluC digestion of P10. The MALDI-TOF spectrum shows a peak ($[M+H]^+$ 1475.81) corresponding to the peptide ^{82}LDSDARRGKRSSK^{94} (calculated mass 1475.80). Phosphorylation of the P10 C-terminus was confirmed by the presence of the peak $[M+H]^+$ 1555.75 corresponding to ^{82}LDSDARRGKRSSK^{94} + 1P (PO_3^{2-}) (calculated mass 1555.77). This finding suggests that either serine 92 or serine 93 in the peptide ^{82}LDSDARRGKRSSK^{94} is a phospho-acceptor site of the P10 protein. Another peptide, ^{55}IQSILTGDIVPDLPDSLKPKLKSQAFE^{81}, was also examined using MALDI-TOF but did not reveal a form consistent with phosphorylation of serine 70 (data not shown).

3. Temporal analysis of P10 mutant structures by confocal microscopy

Recombinant viruses were generated containing serine-alanine mutations at positions 92 and 93 or at both residues within P10 (Figure 3). These viruses, AcP10^{S9293A}, AcP10^{S92A}, AcP10^{S93A} and a control AcP10^{wt} were used to infect TN368 cells at an MOI of 10, which were examined subsequently using confocal microscopy. The images were obtained from a number of different cells at each time-point and are representative; the heterogeneous nature of the TN368 cell line was taken into account during the analysis.

Figure 4 shows P10 mutant and control structures at 72- (Fig. 4, upper panels) and 96 hpi (Fig. 4, lower panels) when under control of the *polh* promoter. The P10 structures of AcP10^{wt} exhibited the same profile as the wild-type AcMNPV structures at 72- and 96 hpi (compare Figure 4, left hand panels with Figure 1); both cytoplasmic filaments and peri-nuclear tubules were present.

Similar to the wild-type AcMNPV infection (Figure 1), a few cytoplasmic filaments were detached at 72 hpi; however, by 96 hpi all filaments appeared detached and a distinctive P10 tubular structure surrounding the nucleus in a ring-like form was visible at both 72- and 96 hpi. This structure remained intact at 96 hpi and disjointedfrom the cytoplasmic filaments.

The P10 mutant structures of $AcP10^{S92A}$ were similar to those of $AcP10^{wt}$ and developed at the same time (Figure 4). However, the P10 mutant structures of $AcP10^{S93A}$ and $AcP10^{S9293A}$ revealed conformational differences when compared to the control $AcP10^{wt}$ (Figure 4). The ring-like form of P10 perinuclear tubule is absent and is replaced by thin filaments surrounding the nucleus at 96hpi in these mutants. The mutant cytoplasmic filaments were disorganised, and displayed thinner and rigid conformation at 72- and 96 hpi indicating a structural aberration. In addition, these filaments displayed a delay in detachment from the cell nucleus compared to those from $AcP10^{wt}$ infection (Figure 4) or wild-type AcMNPV (Figure 1). These results suggest that a single mutation of the P10 residue, serine 93, affects the organisation of P10 filaments and consequently disrupts their detachment from the nucleus. It does not, however, completely abolish the detachment as some filaments were detached from the nucleus at both 72- and 96 hpi. The detachment was further analysed in relation to the microtubules. The co-localisation of P10 mutant structures with microtubules was compared to that of the wildtype (Figure 4).

4. Mass spectrometric analysis of the C-terminus of P10 mutants

MALDI-TOF mass spectrometry was employed to identify the site of phosphorylation in AcMNPV P10. This was done by analysing the phosphorylation associated mass shifts in the mutant and the wild-type P10. The consensus sequence for PKA includes the motif XRXS(T)X (R: Arginine, K: Lysine, X: any amino acid, S: Serine, T: Threonine) (25) and serine 93 of P10

fulfils this requirement (last 5 residues of P10 are KRSS*K; *serine 93). Therefore, serine 93 mutant of P10 was selected for mass spectrometric analysis. Furthermore, P10 C-terminus has been shown to be efficiently phosphorylated by PKA (15).

The MALDI-TOF analysis was performed following infection of *T. ni* cells with recombinant viruses $AcP10^{S93A}$ and $AcP10^{wt}$ at an MOI of 10. The MALDI-TOF spectrum was analysed for peaks corresponding to the C-terminal peptides containing serine 93 (unmodified) or alanine 93 (mutant) residues from $AcP10^{wt}$ and $AcP10^{S93A}$, respectively.

Figure 5 shows the MALDI-TOF spectra containing the mass-to-charge ratio (m/z) peaks corresponding to the C-terminal peptide ^{82}LDSDARRGKRS(S/A)K^{94}, a product of the endoproteinase GluC digestion of P10. In these spectra, the labelled m/z peaks correspond to the P10 C-terminal peptide ^{82}LDSDARRGKRSSK^{94} ($[M+H]^+$ 1475.81, calculated mass 1475.80) or ^{82}LDSDARRGKRSAK^{94} ($[M+H]^+$ 1459.85, calculated mass 1459.81). Phosphorylation of the P10 C-terminal peptide from $AcP10^{wt}$ is evident by the presence of the peak $[M+H]^+$ 1555.75 corresponding to the peptide ^{82}LDSDARRGKRSSK^{94} + 1P (PO_3^{2-}), calculated mass 1555.77. However, in the spectra of the P10 mutant peptide from $AcP10^{S93A}$, no peak is detected at 1539.81, the mass of phosphorylated peptide ^{82}LDSDARRGKRSAK^{94} + 1P (PO_3^{2-}).

These data confirm, by exclusion, that the P10 residue serine 93, and not serine 92, is the substrate residue for a kinase. The presence of the phosphorylated P10 peptide from $AcP10^{wt}$ provides further evidence of phosphorylation in native P10.

5. Circular Dichroism

The Circular dichroism (CD) profile of a protein varies with the different secondary structure elements or folds. Circular dichroism was, therefore, used to analyse the secondary structure of wild-type P10 and its serine 93 mutant in order to determine whether phosphorylation may affect secondary structure characteristics.

Purified protein samples were prepared for CD spectroscopy using the recombinant viruses AcFBU-His-P10^{wt} and AcFBU-His-P10^{S93A} encoding His-tagged wild-type and mutant (serine 93) P10 respectively (Figure 3). The CD profile of the wild-type P10 showed minima at 221 nm and at 208 nm; the serine 93 mutant, at 228.5 nm and at 205-215 nm (Figure 6). To determine the secondary structure of the serine 93 mutant and wild-type P10 from the CD spectra, deconvolution analysis of the spectra was performed using a linear combination of CD spectrum or LINCOMB method. This method uses an algorithm based on a least-squares fit and a set of reference spectra (23). For the P10 CD spectra analysis, the set comprised of typical CD curves of α-helix, β-pleated sheet (antiparallel), β-turns, disordered protein, and aromatic/disulphide (or non-peptide).

Deconvolution of the P10 wild-type spectrum showed that the protein comprised of α-helix (47.86%) followed by β-turns (32.09%) while the remaining structure was random coil (20.05%). In comparison, the P10 serine 93 mutant revealed slightly reduced content of α-helix (43.31%) and higher content of β-turns (37.79%). The percentage content of random coil in the two samples did not vary.

Discussion

The formation of P10 cytoskeletal-like structures during AcMNPV infection has been established in a number of previous studies (12–14). In this study, examination of P10 structures at 48-, 72- and 96 hpi using confocal microscopy revealed that they undergo a transition during this period of the AcMNPV infection cycle. The P10 tubular structure, which surrounded the host nucleus, was present from 48 hpi and developed into a discrete ring-like form disjointed from the P10 cytoplasmic filaments by 96 hpi. In contrast, the P10 cytoplasmic filaments became detached and disintegrated by 96 hpi. Previously (14), these structures were described at 48 hpi. To better understand the significance of P10 structures during infection, we analysed how these structures transform until a very late time point such as 96 hpi when cells undergo lysis. These results are also consistent with the findings from the pulse-labelling experiments (24) that reported high level synthesis of P10 from 33 to 99 hpi. The fact that P10 continues to form structures in the host cell following the viral replication cycle is one of the key findings of this study. This phenomenon is indeed indicative of the requirement of this protein at this post-replication stage.

Phosphorylation of P10 has been postulated in a number of previous studies (12, 14, 15); however, there was no evidence to suggest that the phenomenon occurred in the wild-type virus infection. Herein, we report phosphorylation of P10 in wild-type AcMNPV infection at 7hpi using mass spectrometric analysis of P10 (Figure 2); however, this was a small proportion in comparision to the non-phosphorylated peptide. But considering technical limitations, the amount of phsophorylated peptide observed in this assay may not be truly reflective of the total amount of phosphorylated P10 present during infection. MALDI-TOF analysis of P10 mutants found that the C-terminal residue, serine 93, is the site of phosphorylation (Figure 5). This

phosphorylation site is conserved in P10 sequences from six members of alphabaculoviruses and there are potential phosphorylation sites in the C-terminal basic domain of P10 whose distribution is highly conserved in alphabaculovirus P10 homologues (7). Baculoviruses are known to encode several kinases that include serine/threonine kinases PK-1 and PK-2, which are expressed very-late or late respectively (26, 27). Thus, it is likely that P10 is phosphorylated by PK-1 or -2 encoded by the virus.

Phosphorylated P10 was also found in the cells infected with the recombinant viruses AcP10^{wt}. This suggested that the dynamics of P10 phosphorylation in the recombinant viruses were comparable to the wild-type infection and thus unaffected by the use of the polyhedrin promoter. Phosphorylation was inhibited in the mutant P10 from cells infected with the recombinant virus AcP10^{S93A} in which the phosphorylation site, serine 93, was substituted with alanine.

P10 structures of AcP10^{S93A} and AcP10^{S9293A} revealed significant differences compared to the wild-type control virus AcP10^{wt} (Figure 4) and wild-type virus (Figure 1). Mutation of the phosphorylation site serine 93 resulted in aberrant formation of the P10 peri-nuclear tubules; it also affected the conformation of the cytoplasmic filaments. Therefore, it is very likely that phosphorylation of the P10 C-terminus facilitates aggregation of P10 in order to form the much distinctive tubular structures in the final stages of the infection. The timing of P10 phosphorylation (72hpi) observed in the mass spectrometry data also correlates with the formation of these structures. The serine 93 mutants also showed a delay in the detachment of filaments from the nucleus suggesting that the aggregated filaments facilitated this process. Indeed phosphorylation modulates the aggregation propensity of several proteins and peptides (28–30); these include tau, synuclein and peptide model systems. Aggregation of self-assembling

proteins is particularly regulated by phosphorylation (31) and this may also be true for P10, which also self-assembles (32).

The changes observed in the P10 mutant structures are unlikely to be caused by the substitution of serine with alanine at position 93 as both alanine and serine have neutral pH. Additionally, the observation that the P10 structures of the serine 92 mutant are similar to wild-type P10 structures further confirms that a single substitution of serine with alanine, in close proximity of the penultimate residue, does not have any observable influence on protein conformation.

This study analysed the secondary structure of wild-type and serine 93 mutant P10 using the CD spectroscopy. No previous work has been done to reveal the secondary structure of P10. A reduction in the α-helical content of the P10 was observed upon mutation of serine 93. Although not analysed, the serine 92 mutant most likely retained the wildtype conformation as no differences were observed in the P10 structures with confocal microscopy. Moreover, results from the secondary structure prediction software PSIPRED showed no differences in the secondary structure of P10 upon substitution of serine 92 or serine 93 with alanine. Therefore, it is unlikely that the substitution of serine 92 or 93 with alanine produced a significant change in the secondary structure of P10 unless there is a post-translational modification of the protein. Thus, the change in secondary structure could be a result of the addition of a phosphate moiety to a protein that is known to affect the electrostatic forces in a protein determining its folding. The type and extent of change in the folding varies with the location of the phosphorylation and is not entirely predictable. It is likely that the phosphorylation of the P10 penultimate residue plays a role in the stabilisation of the entire protein.

500 Taken together, the results of this study support the hypothesis that the phosphorylation of P10 at
501 the C-terminus regulates its structural organisation. This phenomenon could be involved in
502 multiple roles of P10 during virus infection. The P10 peri-nuclear tubules surround the polyhedra
503 inside the cell nucleus, which indicates that they may have a protective role in the terminal stages
504 of infection. These tubules may also stabilise the host nucleus to allow complete maturation of
505 polyhedra to take place. Without the tubules, the polyhedra may be susceptible to digestion by
506 viral cathepsin that is activated upon cell death. (33). This could also explain the results from an
507 early study by Gross *et al*. (10) in which the periphery of the polyhedra were affected upon
508 deletion of the *p10* gene. The phosphorylation driven aggregation of P10 cytoplasmic filaments
509 may also be involved in timely destruction of the host cell to release the viral enzymes. This is
510 consistent with the study in which deletion of P10 delayed the release of chitinase by 24 hours
511 (33).
512
513 Microtubule associated proteins (MAPs) such as tau have a basic C-terminus that interacts with
514 the negatively charged residues in tubulin (34). Phosphorylation of the MAP tau allows it to
515 dissociate from the MTs because of the negative charge introduced by phosphorylation (35).
516 Furthermore, aggregation of tau is also faciliated by phosphorylation (36). The C-terminus of
517 P10, which is also the site of phosphorylation, is basic in nature since it is rich in lysine and
518 arginine residues. Similar to the tau protein, the interaction of P10 with MTs may be facilitated
519 through these basic residues and phosphorylation of P10 may influence its affinity for MTs and
520 self-aggregation preoperties. Although no differences were observed in the co-alignment of
521 mutant filaments with MTs in comparison to the wild-type, the mutants showed rigid
522 conformation and a delayed detachment from the nucleus (results not shown). These
523 observations could be the result of the altered affinity of P10 structures for MTs upon the

inhibition of phosphorylation. Testing this model could explain one of the mechanisms through which baculoviruses are able to take control of the host cytoskeleton.

Acknowledgements

The authors are grateful to Professor John Runions (Oxford Brookes University) and Dr David Staunton (University of Oxford) for their technical expertise with confocal microscopy and circular dichroism, respectively. The latter work was performed at University of Oxford with a research grant from the Santander Group.

References

1. **Federici BA**. 1986. Ultrastructure of baculoviruses, p. 61–88. *In* Granados, RR, Federici, BA (eds.), The Biology of Baculoviruses. CRC Press, Boca Raton, Fla.

2. **Vaughn JL, Faulkner P**. 1963. Susceptibility of an insect tissue culture to infection by virus preparations of the nuclear polyhedrosis of the silkworm (bombyx mori l.). Virology **20**:484–489.

3. **Summers MD, Volkman LE**. 1976. Comparison of biophysical and morphological properties of occluded and extracellular nonoccluded baculovirus from in vivo and in vitro host systems. J Virol **17**:962–972.

4. **Bilimoria S**. 1986. Taxonomy and identification of baculoviruses, p. 37–59. *In* Granados, R, Federeci, B (eds.), The biology of baculoviruses. CRC Press, Boca Raton, Fla.

5. **Thiem SM, Miller LK**. 1990. Differential gene expression mediated by late, very late and hybrid baculovirus promoters. Gene **91**:87–94.

6. **Rohel DZ, Cochran MA, Faulkner P**. 1983. Characterization of two abundant mRNAs of Autographa californica nuclear polyhedrosis virus present late in infection. Virology **124**:357–365.

7. **Carpentier DCJ, King LA**. 2009. The long road to understanding the baculovirus P10 protein. Virol Sin **24**:227–242.

8. **Vlak JM, Klinkenberg FA, Zaal KJ, Usmany M, Klinge-Roode EC, Geervliet JB, Roosien J, van Lent JW**. 1988. Functional studies on the p10 gene of Autographa californica nuclear polyhedrosis virus using a recombinant expressing a p10-beta-galactosidase fusion gene. J Gen Virol **69 (Pt 4)**:765–776.

9. **Williams GV, Rohel DZ, Kuzio J, Faulkner P**. 1989. A cytopathological investigation of Autographa californica nuclear polyhedrosis virus p10 gene function using insertion/deletion mutants. J Gen Virol **70 (Pt 1)**:187–202.

10. **Gross CH, Russell RL, Rohrmann GF**. 1994. Orgyia pseudotsugata baculovirus p10 and polyhedron envelope protein genes: analysis of their relative expression levels and role in polyhedron structure. J Gen Virol **75 (Pt 5)**:1115–1123.

11. **Summers MD, Arnott HJ**. 1969. Ultrastructural studies on inclusion formation and virus occlusion in nuclear polyhedrosis and granulosis virus-infected cells of Trichoplusia ni (Hübner). J Ultrastruct Res **28**:462–480.

12. **Quant-Russell RL, Pearson MN, Rohrmann GF, Beaudreau GS**. 1987. Characterization of baculovirus p10 synthesis using monoclonal antibodies. Virology **160**:9–19.

13. **Patmanidi AL, Possee RD, King LA**. 2003. Formation of P10 tubular structures during AcMNPV infection depends on the integrity of host-cell microtubules. Virology **317**:308–320.

14. **Carpentier DCJ, Griffiths CM, King LA**. 2008. The baculovirus P10 protein of Autographa californica nucleopolyhedrovirus forms two distinct cytoskeletal-like structures and associates with polyhedral occlusion bodies during infection. Virology **371**:278–291.

15. **Cheley S, Kosik KS, Paskevich P, Bakalis S, Bayley H**. 1992. Phosphorylated baculovirus p10 is a heat-stable microtubule-associated protein associated with process formation in Sf9 cells. J Cell Sci **102 (Pt 4)**:739–752.

16. **Luckow VA, Summers MD**. 1988. Trends in the Development of Baculovirus Expression Vectors. Nat Biotechnol **6**:47–55.

17. **Vaughn JL, Goodwin RH, Tompkins GJ, McCawley P**. 1977. The establishment of two cell lines from the insect Spodoptera frugiperda (Lepidoptera; Noctuidae). In Vitro **13**:213–217.

18. **Granados RR, Guoxun L, Derksen ACG, McKenna KA**. 1994. A new insect cell line from Trichoplusia ni (BTI-Tn-5B1-4) susceptible to Trichoplusia ni single enveloped nuclear polyhedrosis virus. Journal of invertebrate pathology **64**:260–266.

19. **Hink WF**. 1970. Established insect cell line from the cabbage looper, Trichoplusia ni. Nature **226**:466–467.

20. **Possee RD**. 1986. Cell-surface expression of influenza virus haemagglutinin in insect cells using a baculovirus vector. Virus Res **5**:43–59.

21. **Vandeyar MA, Weiner MP, Hutton CJ, Batt CA**. 1988. A simple and rapid method for the selection of oligodeoxynucleotide-directed mutants. Gene **65**:129–133.

22. **King LA, Possee RD**. 1992. The baculovirus expression system : a laboratory guide. Chapman & Hall, London; New York, N.Y.

23. **Perczel A, Park K, Fasman GD**. 1992. Analysis of the circular dichroism spectrum of proteins using the convex constraint algorithm: a practical guide. Anal Biochem **203**:83–93.

24. **Smith GE, Vlak JM, Summers MD**. 1983. Physical Analysis of Autographa californica Nuclear Polyhedrosis Virus Transcripts for Polyhedrin and 10,000-Molecular-Weight Protein. J Virol **45**:215–225.

25. **Hennrich ML, Marino F, Groenewold V, Kops GJPL, Mohammed S, Heck AJR**. 2013. Universal quantitative kinase assay based on diagonal SCX chromatography and stable isotope dimethyl labeling provides high-definition kinase consensus motifs for PKA and human Mps1. J Proteome Res **12**:2214–2224.

26. **Reilly LM, Guarino LA**. 1994. The pk-1 gene of Autographa californica multinucleocapsid nuclear polyhedrosis virus encodes a protein kinase. J Gen Virol **75 (Pt 11)**:2999–3006.

27. **Li Y, Miller LK**. 1995. Expression and functional analysis of a baculovirus gene encoding a truncated protein kinase homolog. Virology **206**:314–323.

28. **Schneider A, Biernat J, von Bergen M, Mandelkow E, Mandelkow EM**. 1999. Phosphorylation that detaches tau protein from microtubules (Ser262, Ser214) also protects it against aggregation into Alzheimer paired helical filaments. Biochemistry **38**:3549–3558.

29. **Paleologou KE, Schmid AW, Rospigliosi CC, Kim H-Y, Lamberto GR, Fredenburg RA, Lansbury PT, Fernandez CO, Eliezer D, Zweckstetter M, Lashuel HA**. 2008. Phosphorylation at Ser-129 but not the phosphomimics S129E/D inhibits the fibrillation of alpha-synuclein. J Biol Chem **283**:16895–16905.

30. **Kühnle H, Börner HG**. 2009. Biotransformation on polymer-peptide conjugates: a versatile tool to trigger microstructure formation. Angew Chem Int Ed Engl **48**:6431–6434.

31. **Valette NM, Radford SE, Harris SA, Warriner SL**. 2012. Phosphorylation as a tool to modulate aggregation propensity and to predict fibril architecture. Chembiochem **13**:271–281.

32. **Alaoui-Ismaili MH, Richardson CD**. 1998. Insect virus proteins (FALPE and p10) self-associate to form filaments in infected cells. J Virol **72**:2213–2223.

33. **Thomas CJ, Brown HL, Hawes CR, Lee BY, Min MK, King LA, Possee RD**. 1998. Localization of a baculovirus-induced chitinase in the insect cell endoplasmic reticulum. J Virol **72**:10207–10212.

34. **Morris M, Maeda S, Vossel K, Mucke L**. 2011. The many faces of tau. Neuron **70**:410–426.

35. **Bramblett GT, Goedert M, Jakes R, Merrick SE, Trojanowski JQ, Lee VM**. 1993. Abnormal tau phosphorylation at Ser396 in Alzheimer's disease recapitulates development and contributes to reduced microtubule binding. Neuron **10**:1089–1099.

36. **Alonso A, Zaidi T, Novak M, Grundke-Iqbal I, Iqbal K**. 2001. Hyperphosphorylation induces self-assembly of tau into tangles of paired helical filaments/straight filaments. Proc Natl Acad Sci U S A **98**:6923–6928.

Figure Legends

Figure 1. Temporal changes in the P10 structures during AcMNPV infection of TN368 cells. (A) The amino acid sequence of AcMNPV P10 reveals three distinct regions, a coiled-coil domain at the N-terminus (blue residues), a proline-rich region in the variable region (green residues) and a positively charged basic region at the C-terminus (red residues; R: Arginine, K: Lysine). Amino acid residues of the heptad repeat in the coiled-coil region are denoted as *abcdefg*, in which *a* and *d* are hydrophobic whereas *e* and *g* are charged residues. (B) Wildtype-infected TN368 cells were analysed at 48-, 72- and 96 hpi using confocal laser scanning microscopy. Cells were stained with anti-P10- and Alexa Fluor 488 antibody to visualise P10 (green) and with anti-α-Tubulin- and Alexa Fluor 568 antibody to visualise MTs (red). P10 and α-Tubulin channels were merged to show co-alignment. Position of OB-filled nucleus is shown in the bright field images. At 48- and 72 hpi, P10 filaments were co-aligned with MTs and spanned the host cytoplasm; bundling of these filaments was evident at 72 hpi. P10 also formed peri-nuclear tubular structures that were present from 48 hpi and most developed at 96 hpi. The P10 cytoplasmic filaments appeared detached from the peri-nuclear tubule and partially disintegrated at 96 hpi. Scale bars, 30 μm.

Figure 2. MALDI-TOF mass spectrometric analysis of the P10 C-terminus. The AcMNPV P10 protein was harvested at 72 hpi and digested with endoproteinase GluC to cleave peptide bonds C-terminal to glutamic acid residues. The peptide products were analysed by MALDI-TOF MS (UltraflexTM, Bruker Daltonics) in linear mode. Image shows a portion of the spectrum containing the peptides of interest from P10 C-terminus. The x-axis represents mass divided by charge (m/z) and the y-axis represents absolute intensity. Peaks with m/z values of 1475.81 and 1555.75 corresponded to the non- and mono-phosphorylated states of the P10 C-terminus peptide ^{82}LDSDARRGKRSSK^{94}.

Figure 3. Construction of recombinant viruses. (A) Wild-type or mutant *p10* flanked by *Xba*I and *Xma*I restriction sites was inserted downstream of the polyhedrin promoter in the transfer vector pBacPAK8. Recombinant baculoviruses were made by allowing homologous recombination of the transfer vector and *flash*BACULTRA. Four viruses were constructed; in single mutants, AcP10^{S92A} and AcP10^{S93A}, serine 92 and 93 were mutated to alanine respectively. In the double mutant, AcP10^{S9293A}, both serine 92 and 93 were mutated to alanine. AcP10^{wt} contained the wild-type *p10*. (B) pAcUW2B was used to construct the His-tagged wild-type and mutant *p10* encoding viruses. This vector included a complete *polh* gene. The P10 fragment was inserted downstream of the P10 promoter in pAcUW2B using the *Pst*I and *Spe*I restriction sites. Six histidine residues followed by the TEV cleavage site residues were added at the N-terminus. Two recombinant viruses were constructed by co-transfecting pAcUW2B modified vectors with *flash*BACULTRA: Ac-His-P10^{wt}, containing wild-type *p10* gene and mutant Ac-His-P10^{S93A} Displayed genes are not to scale.

Figure 4. Analysis of wild-type and mutant P10 structures. TN368 cells were infected with AcP10^{wt}, AcP10^{S92A}, AcP10^{S93A} or AcP10^{S9293A} and then fixed at 72- and 96 hpi. P10 structures were visualised by anti-P10- and Alexa Fluor 488 antibody; microtubules(red) were visualised by anti-αTubulin- and Alexa Fluor 568 antibody. P10 and α-Tubulin channels were merged to show co-alignment.At 72 hpi, cells infected with AcP10^{wt} or AcP10^{S92A} showed both P10 peri-nuclear tubules (NT) and cytoplasmic filaments (CF). By 96 hpi, the peri-nuclear tubules had matured and most cytoplasmic filaments were detached from the central tubule. Cells infected with AcP10^{S93A} or AcP10^{S9293A} lacked peri-nuclear tubules and displayed rigid and angular cytoplasmic filaments that were not fully detached from the nucleus. Images are representative. Scale bars, 30 μm.

Figure 5. MALDI-TOF mass spectrometric analysis of the P10 peptides from AcP10^{wt} and AcP10^{S93A}. In-gel digestion of P10 protein (separated by SDS-PAGE) from AcP10^{wt} and AcP10^{S93A} was carried out with endoproteinase GluC; this cleaved peptide bonds C-terminal to glutamic acid residues in ammonium carbonate buffer. The peptide fragments were analysed by MALDI-TOF MS (Ultraflex^{TM}, Bruker Daltonics) in linear mode. Image shows a portion of the spectrum containing the P10 C-terminal peptides of interest. The x-axis represents mass-to-charge ratio (m/z) and the y-axis represents absolute intensity as measured by the detector. The top panel shows the MALDI-TOF spectrum of the P10 C-terminal peptide from AcP10^{wt}, in which wild-type P10 expression was driven by the polyhedrin gene promoter. The MALDI-TOF spectrum shows peaks with m/z values of 1475.81 and 1555.75 that corresponded to the non- and mono-phosphorylated states of the P10 peptide ^{82}LDSDARRGKRSSK^{94}. The bottom panel

shows the MALDI-TOF spectrum of the P10 peptide from AcP10^{S93A}. In this recombinant virus, the P10 residue serine 93 was mutated to alanine and the mutant expression was driven by the *polh* promoter. The MALDI-TOF spectrum shows a signal at $[M+H]^+$ 1459.85 corresponding to the peptide ^{82}LDSDARRGKRSAK^{94}, however, no phosphorylated form of this peptide was observed (no signal at m/z 1539).

Figure 6. Secondary structure of wildtype P10 and its serine 93 mutant. Spectra were averaged from 4 to 16 scans in the wavelength range 260–190 nm. CD was measured in ellipticity units, millidegrees (mdeg). The CD spectra of the serine 93 mutant and wildtype P10 revealed differences in the minima. Table shows the percentage of different secondary structures in the two proteins following LINCOMB analysis of spectra.

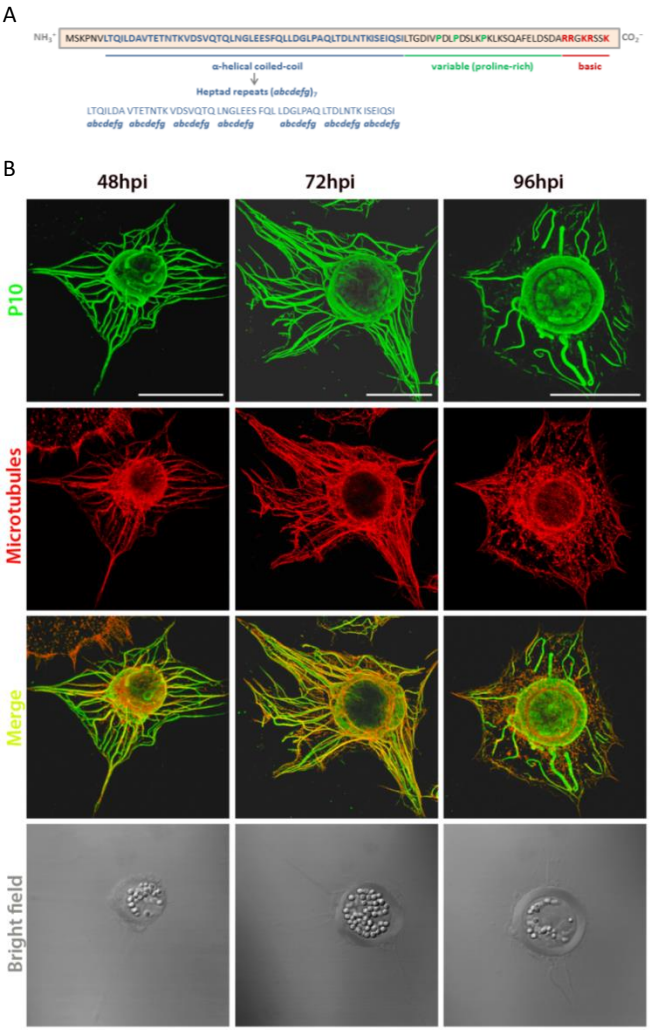

Figure 1. Temporal changes in the P10 structures during AcMNPV infection of TN368 cells. (A) The amino acid sequence of AcMNPV P10 reveals three distinct regions, a coiled-coil domain at the N-terminus (blue residues), a proline-rich region in the variable region (green residues) and a positively charged basic region at the C-terminus (red residues; R: Arginine, K: Lysine). Amino acid residues of the heptad repeat in the coiled-coil region are denoted as *abcdefg*, in which *a* and *d* are hydrophobic whereas *e* and *g* are charged residues. (B) Wildtype-infected TN368 cells were analysed at 48-, 72- and 96 hpi using confocal laser scanning microscopy. Cells were stained with anti-P10- and Alexa Fluor 488 antibody to visualise P10 (green) and with anti-α-Tubulin- and Alexa Fluor 568 antibody to visualise MTs (red). P10 and α-Tubulin channels were merged to show co-alignment. Position of OB-filled nucleus is shown in the bright field images. At 48- and 72 hpi, P10 filaments were co-aligned with MTs and spanned the host cytoplasm; bundling of these filaments was evident at 72 hpi. P10 also formed peri-nuclear tubular structures that were present from 48 hpi and most developed at 96 hpi. The P10 cytoplasmic filaments appeared detached from the peri-nuclear tubule and partially disintegrated at 96 hpi. Scale bars, 30 µm.

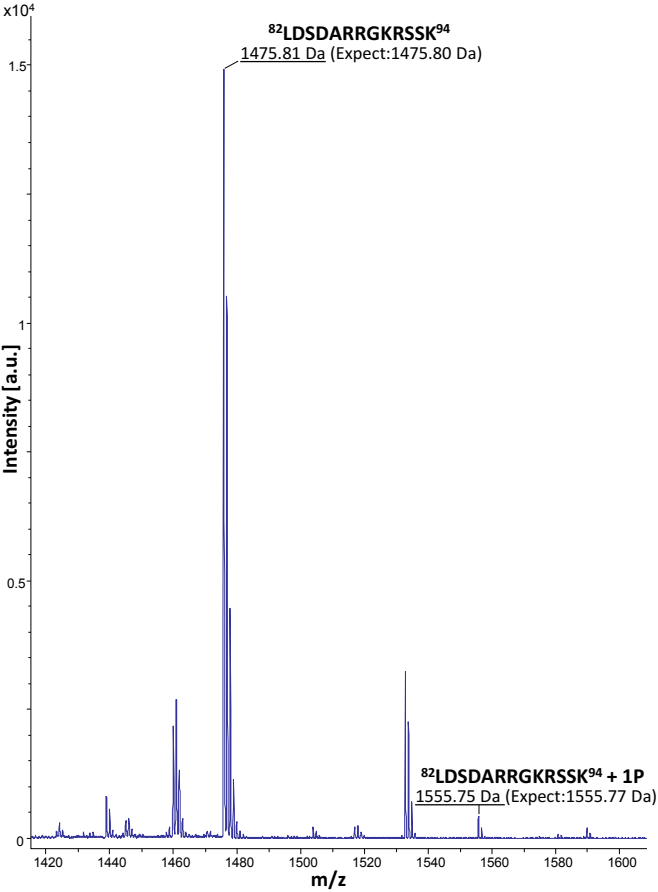

Figure 2. MALDI-TOF mass spectrometric analysis of the P10 C-terminus. The AcMNPV P10 protein was harvested at 72 hpi and digested with endoproteinase GluC to cleave peptide bonds C-terminal to glutamic acid residues. The peptide products were analysed by MALDI-TOF MS (UltraflexTM, Bruker Daltonics) in linear mode. Image shows a portion of the spectrum containing the peptides of interest from P10 C-terminus. The x-axis represents mass divided by charge (m/z) and the y-axis represents absolute intensity. Peaks with m/z values of 1475.81 and 1555.75 corresponded to the non- and mono-phosphorylated states of the P10 C-terminus peptide ^{82}LDSDARRGKRSSK^{94}.

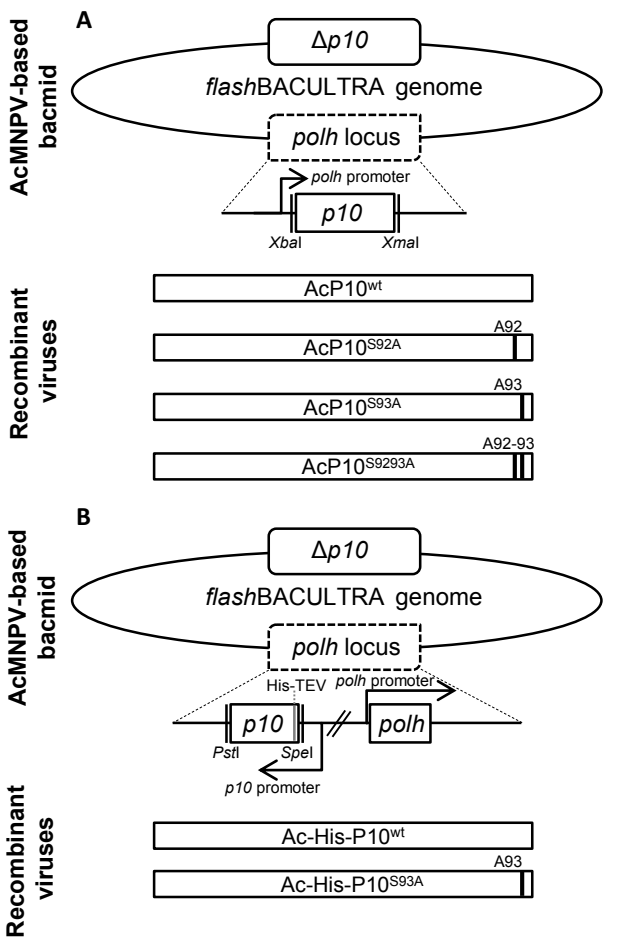

Figure 3. Construction of recombinant viruses. (A) Wild-type or mutant *p10* flanked by *Xba*I and *Xma*I restriction sites was inserted downstream of the polyhedrin promoter in the transfer vector pBacPAK8. Recombinant baculoviruses were made by allowing homologous recombination of the transfer vector and *flash*BACULTRA. Four viruses were constructed; in single mutants, AcP10^{S92A} and AcP10^{S93A}, serine 92 and 93 were mutated to alanine respectively. In the double mutant, AcP10^{S9293A}, both serine 92 and 93 were mutated to alanine. AcP10^{wt} contained the wild-type *p10*. (B) pAcUW2B was used to construct the His-tagged wild-type and mutant *p10* encoding viruses. This vector included a complete *polh* gene. The P10 fragment was inserted downstream of the P10 promoter in pAcUW2B using the *Pst*I and *Spe*I restriction sites. Six histidine residues followed by the TEV cleavage site residues were added at the N-terminus. Two recombinant viruses were constructed by co-transfecting pAcUW2B modified vectors with *flash*BACULTRA: Ac-His-P10^{wt}, containing wild-type *p10* gene and mutant Ac-His-P10^{S93A} Displayed genes are not to scale.

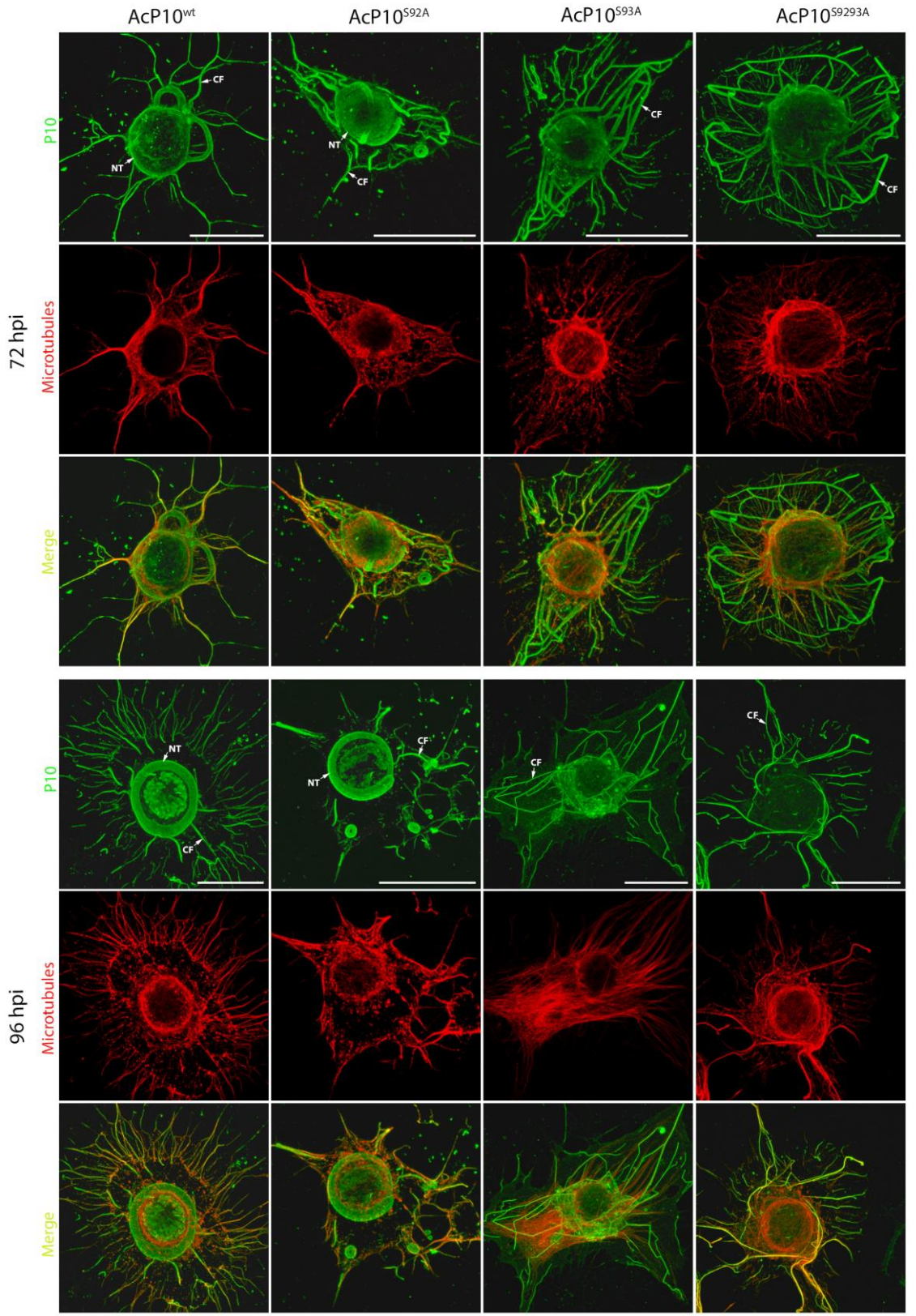
AcP10wt
AcP10S92A
AcP10S93A
AcP10S9293A
72 hpi
96 hpi
P10
Microtubules
Merge
CF
NT

Figure 4. Analysis of wild-type and mutant P10 structures. TN368 cells were infected with AcP10^{wt}, AcP10^{S92A}, AcP10^{S93A} or AcP10^{S9293A} and then fixed at 72- and 96 hpi. P10 structures were visualised by anti-P10- and Alexa Fluor 488 antibody; microtubules (red) were visualised by anti-αTubulin- and Alexa Fluor 568 antibody. P10 and α-Tubulin channels were merged to show co-alignment. At 72 hpi, cells infected with AcP10^{wt} or AcP10^{S92A} showed both P10 peri-nuclear tubules (NT) and cytoplasmic filaments (CF). By 96 hpi, the peri-nuclear tubules had matured and most cytoplasmic filaments were detached from the central tubule. Cells infected with AcP10^{S93A} or AcP10^{S9293A} lacked peri-nuclear tubules and displayed rigid and angular cytoplasmic filaments that were not fully detached from the nucleus. Images are representative. Scale bars, 30 μm.

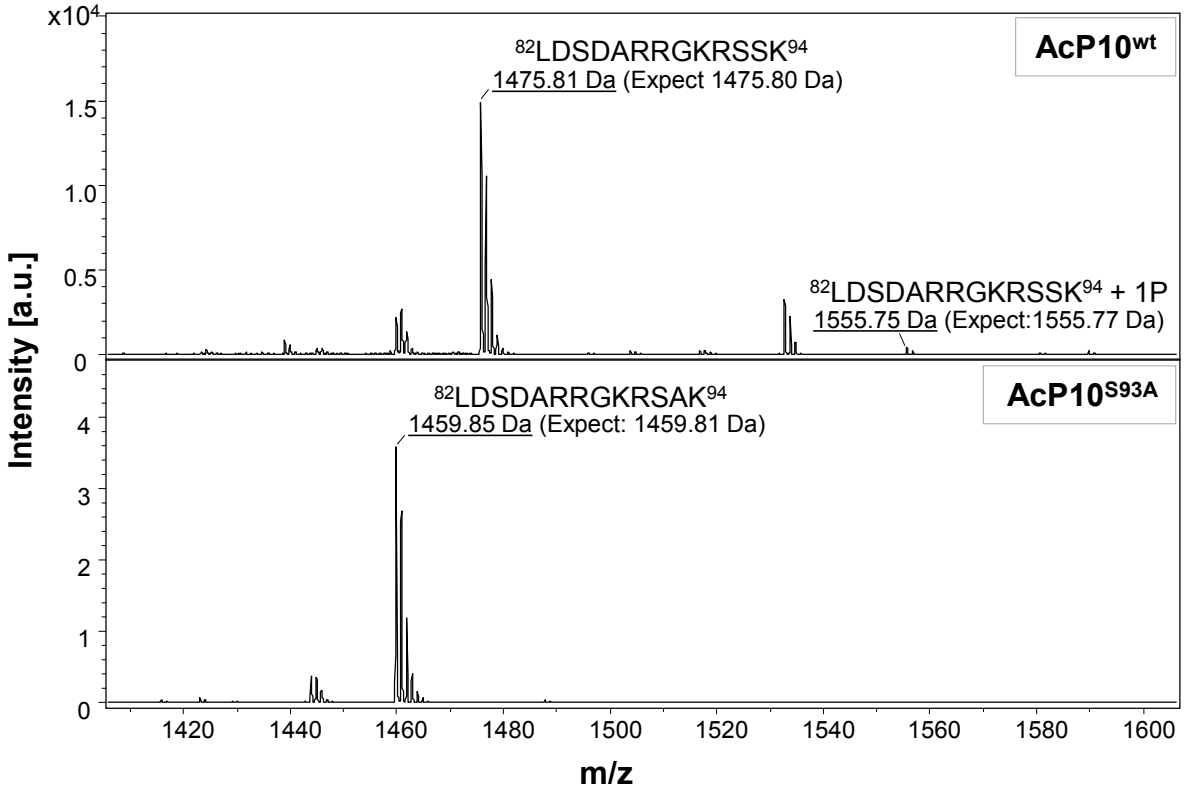

Figure 5. MALDI-TOF mass spectrometric analysis of the P10 peptides from AcP10^{wt} and AcP10^{S93A}. In-gel digestion of P10 protein (separated by SDS-PAGE) from AcP10^{wt} and AcP10^{S93A} was carried out with endoproteinase GluC; this cleaved peptide bonds C-terminal to glutamic acid residues in ammonium carbonate buffer. The peptide fragments were analysed by MALDI-TOF MS (Ultraflex^{TM}, Bruker Daltonics) in linear mode. Image shows a portion of the spectrum containing the P10 C-terminal peptides of interest. The x-axis represents mass-to-charge ratio (m/z) and the y-axis represents absolute intensity as measured by the detector. The top panel shows the MALDI-TOF spectrum of the P10 C-terminal peptide from AcP10^{wt}, in which wild-type P10 expression was driven by the polyhedrin gene promoter. The MALDI-TOF spectrum shows peaks with m/z values of 1475.81 and 1555.75 that corresponded to the non- and mono-phosphorylated states of the P10 peptide ^{82}LDSDARRGKRSSK^{94}. The bottom panel shows the MALDI-TOF spectrum of the P10 peptide from AcP10^{S93A}. In this recombinant virus, the P10 residue serine 93 was mutated to alanine and the mutant expression was driven by the *polh* promoter. The MALDI-TOF spectrum shows a signal at $[M+H]^+$ 1459.85 corresponding to the peptide ^{82}LDSDARRGKRSAK^{94}, however, no phosphorylated form of this peptide was observed (no signal at m/z 1539).

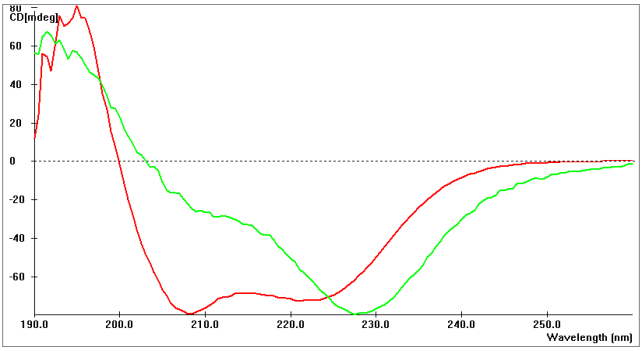

Protein	α-helix (%)	β-Turn (%)	Random coil (%)	Error (SD)
P10 wild-type	47.86	32.09	20.05	0.950
P10 mutant (S93A)	43.31	37.79	18.90	0.855

Figure 6. Secondary structure of wildtype P10 and its serine 93 mutant. Spectra were averaged from 4 to 16 scans in the wavelength range 260–190 nm. CD was measured in ellipticity units, millidegrees (mdeg). The CD spectra of the serine 93 mutant and wildtype P10 revealed differences in the minima. Table shows the percentage of different secondary structures in the two proteins following LINCOMB analysis of spectra.